

Status of CME Search Before Isobar Collisions and Methods of Blind Analysis From STAR

Prithwish Tribedy for the STAR collaboration

Physics Department, Brookhaven National Laboratory, Upton, NY

E-mail: ptribedy@bnl.gov

Abstract. The STAR collaboration is currently pursuing the blind analysis of the data for isobar collisions that was performed at RHIC in the year 2018 to make a decisive test of the Chiral Magnetic Effect (CME). Why is it so difficult to detect signals of CME in the experiment? Do we really understand different sources of background? Why observing similar charge separation between $p/d + A$ and $A + A$ does not stop us from pursuing the search for CME? In this contribution, I attempt to address some of these questions and briefly outline a few recent STAR analyses based on new methods and observables to isolate the possible CME-driven signal and non-CME background contributions at the top RHIC energy. Finally, I describe the procedure for the blind analysis of the isobar data. An outstanding question remains – what happens if we go down in energy? I address this by discussing how the new event-plane detector (EPD) upgrade provides a new capability at STAR towards CME search using the data from the RHIC BES-II program.

1. Introduction

Finding a conclusive experimental signature of the Chiral Magnetic Effect (CME) has become one of the major scientific goals of the heavy-ion physics program at the Relativistic Heavy Ion Collider (RHIC). The existence of CME will be a leap towards an understanding of the QCD vacuum, establishing a picture of the formation of deconfined medium where chiral symmetry is restored and will also provide unique evidence of the strongest known electromagnetic fields created in relativistic heavy-ion collisions [1, 2]. The impact of such a discovery goes beyond the community of heavy-ion collisions and will possibly be a milestone in physics. Also, as it turns out, the remaining few years of RHIC run and analysis of already collected data probably provides the last chance for dedicated CME searches in heavy-ion collisions in the foreseeable future.

Over the past years significant efforts from the STAR as well as other collaborations have been dedicated towards developing new methods and observables to isolate the possible CME-driven signal and non-CME background contributions in the measurements of charge separation across the reaction plane. The most widely studied experimental observable in this context is the γ -correlator, defined as $\langle \cos(\phi_a^\alpha + \phi_b^\beta - 2\Psi_{RP}) \rangle$, where ϕ_a and ϕ_b denote the azimuthal angles of charged particles, α and β are labels for the charge of the particles and Ψ_{RP} is the reaction plane angle [3]. The angle Ψ_{RP} is expected to be strongly correlated to the direction of the magnetic field that enables the γ -correlator to be sensitive to signals of CME, more specifically, CME leads to a difference between same sign (SS, $\alpha = \beta$) and opposite sign (OS, $\alpha \neq \beta$) charge correlations: $\Delta\gamma = \gamma_{OS} - \gamma_{SS}$. The STAR time projection chamber (TPC) has a wide

39 acceptance at mid-rapidity ($|\eta| < 1$) that is used to detect ϕ_a and ϕ_b . And, in STAR the proxy for
40 Ψ_{RP} can be played by: 1) second-order harmonic anisotropy plane Ψ_2 of produced particles at
41 mid-rapidity measured by TPC, 2) the first-order plane due to the spectator neutrons (Ψ_{ZDC})
42 detected by the zero degree calorimeters (ZDC), 3) the forward Ψ_2 plane using the STAR
43 beam beam counter BBCs and 4) very recently using both the first and second-order harmonic
44 anisotropy planes using the forward Event Plane Detector (EPDs). Each of these planes are
45 expected to have more or less measurable correlations to B-field and serves their purpose for
46 the CME search. The first measurement of non-zero $\Delta\gamma$ by the STAR collaboration goes back
47 to [4] where connections to several expectations from CME driven signals of charge separation
48 was identified. Most importantly, the first measurement from STAR [4] also identified several
49 possible contributions from non-CME effects in the experimental observation of non-zero $\Delta\gamma$.
50 Several subsequent measurements from RHIC and LHC have confirmed this observation and
51 provided many additional insights in that direction [4, 5, 6, 7, 8, 9, 10, 11, 12, 13, 14]. In this
52 contribution, I will focus only on RHIC results and refer to LHC results wherever necessary.

53 A major challenge that the γ -correlator faces towards detecting signals of CME involves
54 large non-CME background sources that are: 1) correlated to Ψ_{RP} and 2) independent of Ψ_{RP} .
55 The distinction between the two sources must be carefully noted as they are crucial to the
56 interpretation of several key measurements performed at both RHIC and LHC.

57 **2. Major challenges in isolating background**

58 *2.1. Background sources-I: reaction plane dependent correlations*

59 The possible background contamination due to the first source of Ψ_{RP} dependent correlation was
60 already alluded to in the reference where γ -correlator was first proposed [3]. At that time only
61 neutral resonance particles were identified as the major source of such background albeit thought
62 to be sub-dominant. When a flowing neutral resonance decays it enhances the probability of a
63 pair of opposite sign particles to move together along Ψ_{RP} . Such correlations lead to non-zero
64 magnitudes of $\Delta\gamma$ mimicking CME. In this context it is important to mention that recently a
65 data-driven approach to measure resonance contribution of background has been developed in
66 STAR by studying the invariant mass dependence of $\Delta\gamma$ that we discuss later [15]. Later on, a
67 more severe source of Ψ_{RP} background due to correlated production of a pair of opposite charged
68 particles due to local charge conservation (LCC) was proposed [16]. Parametrically, if v_2 is the
69 elliptic flow and N is the multiplicity the background contribution from resonance and LCC
70 should go as $\Delta\gamma_{\text{bkg}} \sim v_2/N$ [3] that is also verified by many model calculations [17]. Recently,
71 many models that incorporate the same basic picture of particle production conserving charge
72 locally from a flowing neutral matter, are able to very well explain measurements of $\Delta\gamma$ without
73 invoking the physics of CME. Despite the success of background models experimental search of
74 CME continued because of a number of reasons. Model predictions have large systematics since
75 exact mechanism of hadronization is poorly understood, limited constraints from independent
76 measurements are available. Above all, even the most state-of-the art background models fail
77 to explain all qualitative features of the data (e.g. $\Delta\gamma$ in central collisions, see Fig.1). While
78 the models continue to refine their predictive power, over many years this largely lead to a
79 major effort in beating the background sources in the measurement of charge separation along
80 Ψ_{RP} . It is worth to mention that phenomenological predictions based on anomalous viscous
81 hydrodynamics are now available that include both CME signal and background contribution
82 and can be used to test the sensitivity of different observables [18].

83 *2.2. Background sources-II: reaction plane independent correlations*

84 The second major sources of non-CME background to $\Delta\gamma$ arises from reaction plane independent
85 non-flow correlations. The possibility of such background was discussed in the first publication
86 of charge separation from STAR [4]. One possible source of such background was identified to

87 be three-particle correlations induced by mini-jet fragmentation which is known to: 1) influence
 88 the determination of event plane, 2) introduce more opposite charge correlation than same
 89 charge correlations. The combination of these two artifacts are supposed to lead to non-zero
 90 $\Delta\gamma$ and mimic CME signals. In Ref [4], an indication of larger contribution of reaction plane
 91 independent background can already be seen in: 1) the sharp increasing strength of $\Delta\gamma$ towards
 92 peripheral events and, 2) large $\Delta\gamma$ in Cu+Cu than in Au+Au system at the same centrality.
 93 Both observations can be supported by HIJING calculation.

94 **3. Using small systems to estimate data driven background**

95 Small collision systems provide unique data-driven ways to measure charge separation in the
 96 background scenario. This is based on the idea that the direction of B-field is uncorrelated to the
 97 elliptic anisotropy plane of the produced particle with respect to which $\Delta\gamma$ is measured [11, 19].
 98 In low-multiplicity or min-bias collisions of small systems such planes are dominated by non-flow
 99 correlations from di-jets or momentum conservation. However, tell-tale signatures of collectivity
 100 have been observed in high multiplicity events of small collision systems – the origin of which
 101 has been a widely discussed topic in our community. There are a few scenarios that decide
 102 whether the elliptic anisotropy plane measured in the experiment will be: 1) correlated to a
 103 geometric plane of participants if collectivity is due to hydrodynamics flow, 2) uncorrelated or
 104 less correlated to geometric plane if collectivity is due to non-hydrodynamic but other initial
 105 state momentum space correlations, e.g. from CGC or escape mechanism and, 3) dominated by
 106 non-flow from di-jets and momentum conservation if no collectivity is observed [20]. Why is this
 107 important for CME search? It is important as these scenarios determine the nature of non-CME
 108 background that will dominate the measurements of $\Delta\gamma$ in small systems. It is also important to
 109 know what kind of baseline measurement do these small systems provide because our ultimate
 110 goal is to interpret measurements in heavy-ion collisions. For example, in the first scenario
 111 hydrodynamic flow driven background combined with local charge conservation will be the
 112 dominant source, important for heavy-ion measurements in most centralities. For the second and
 113 third scenarios reaction plane independent background will be the dominant source, important
 114 for peripheral and smaller sized heavy-ion collisions. Nevertheless, the expectation is that CME
 115 signal in all such scenarios will be small as the B-field in small collision systems are weakly
 116 correlated to elliptic anisotropy plane other than some specific scenarios like what was discussed
 117 in Ref [21]. So in summary, small systems have the potential to provide baseline measurements
 118 for heavy-ion collisions where CME signals are expected to disappear but different background
 119 sources will be present. The CMS measurement was the first to show that in overlapping
 120 multiplicity $\Delta\gamma$ measurements are quantitatively similar between $p + Pb$ and $Pb + Pb$ [11].
 121 STAR measurements performed in $p + Au$ and $d + Au$ systems show similar and in fact larger
 122 charge separation measured in terms of the scaled quantity $\Delta\gamma/v_2 \times N_{ch}$ than the same in
 123 $Au + Au$ measurements [14]. Such observations are striking as they tell us that a very large
 124 value of $\Delta\gamma$ is expected even for 100% background scenario.

125 The following question is often asked. Does measurement in small systems completely rule out
 126 CME? Why do we still pursue the CME search? There are several reasons for not abandoning
 127 CME search in heavy-ion collisions based on the observations from small collision systems. It
 128 is already known that $\Delta\gamma$ in heavy-ion collisions suffer from major background, the possible
 129 existence of CME driven signal has become more of a quantitative question. Therefore only a
 130 quantitative baseline will serve our purpose. So a better question to ask is whether small system
 131 measurements can provide direct quantitative baseline for heavy-ions. Heavy-ion measurements
 132 for CME search are performed where the system size, multiplicity do not necessarily overlap
 133 with that of small systems. It is not straightforward to extrapolate the quantitative background
 134 baselines for $\Delta\gamma$ into such unknown territories where change of physics is eminent. For example,
 135 $\Delta\gamma$ measured for $N_{ch} = 10$ in $p/d + Au$ maybe a good baseline for $A + A$ at the same multiplicity

136 but may not serve as quantitative baselines for $\Delta\gamma$ in $Au + Au$ at $N_{ch} = 100$. One may try to
 137 make a projection under some working assumptions but that will lead to a qualitative baseline
 138 and defeats the major purpose of using small systems as direct quantitative baselines. This is
 139 where isobar collisions come in – that ensures measurements in two systems with very similar
 140 size and shape are compared. It is also difficult to conclude that the case of CME is ruled out
 141 entirely based on the raw $\Delta\gamma$ measurements between $p/d + Au$ and $Au + Au$. In lieu of which
 142 several variants of $\Delta\gamma$, as well as alternative observable such as R -observable, signed balance
 143 function has been developed to quantify the signals of CME [22, 23]. The measurements based
 144 on R -observable show qualitative difference in $p/d + Au$ and $Au + Au$ [24] – that is discussed
 145 in the following section.

146 4. The way forward

147 With the aforesaid introduction on the challenges to disentangle CME from non-CME
 148 background I would like to now proceed with the possible solutions to overcome such a
 149 problem. Many clever ideas have been proposed and applied to existing data. The general
 150 consensus is that measurement from the isobar collisions (Ru+Ru that has 10 – 18% higher
 151 B-field than Zr+Zr) provides the best solution to this problem. In following sections of this
 152 conference proceedings I would like to mention a few such recent efforts such as: 1) Differential
 153 measurements of $\Delta\gamma$ to identify and quantify backgrounds, 2) measurement of higher order
 154 harmonics of γ -correlator, 3) exploiting the relative charge separation across participant and
 155 spectator planes, 4) the use of R -observable to measure charge separation and 5) the use of
 156 signed balance function. The first three approaches are based on aforementioned three-particle
 157 correlator and the last two employ slightly different approaches to quantify charge separation.
 158 There have been many more developments in the recent times and also many LHC measurements
 159 have been performed but I will specifically focus on these five approaches because they will be
 160 explored with the isobar data. The following five sections describe these procedures in brief with
 161 comments on the outlook for isobar blind analysis.

162 5. Differential measurements of $\Delta\gamma$ to identify and quantify background

163 5.1. Invariant mass dependence of charge separation

164 Differential measurements of $\Delta\gamma$ with invariant mass and relative pseudorapidity provide
 165 interesting prospects to identify and quantify the sources of flow and non-flow driven
 166 backgrounds. The idea to use invariant mass is simple and was first introduced in Ref [25].
 167 Resonances are widely identified by observing structures in the invariant mass spectra of the
 168 decay daughters. Take a pair of opposite sign pions for example, a large fraction of them come
 169 from the neutral resonances that show up in the invariant mass spectrum of $m_{inv}(\pi^+ + \pi^-)$. If we
 170 restrict the analysis to pairs of pions, differential measurements of $\Delta\gamma$ with $m_{inv}(\pi^+ + \pi^-)$ should
 171 also show similar peak like structures if background from neutral resonances dominate the charge
 172 separation. Indeed similar peak structures are observed and a careful analysis is performed by
 173 STAR collaboration to extract the possible fraction of CME signals from measurements [15].
 174 This analysis relies on the assumption that CME signals do not show peak like structures in
 175 $m_{inv}(\pi^+ + \pi^-)$ therefore calls for more theoretical inputs in this direction.

176 5.2. Relative pseudorapidity dependence

177 The relative pseudorapidity dependence of azimuthal correlations are widely studied to identify
 178 sources of long-range components that are dominated by early time dynamics as compared to
 179 late time correlations that are prevented by causality to appear as short-range correlations.
 180 The same can be extended to charge dependent correlations that provides the impetus to
 181 explore the dependence of $\Delta\gamma$ on the pseudorapidity gap between the charge carrying particles
 182 $\Delta\eta_{ab} = |\eta_a - \eta_b|$ in $\langle \cos(\phi_a^\alpha + \phi_b^\beta - 2\Psi_{RP}) \rangle$. Such measurements have been performed in STAR

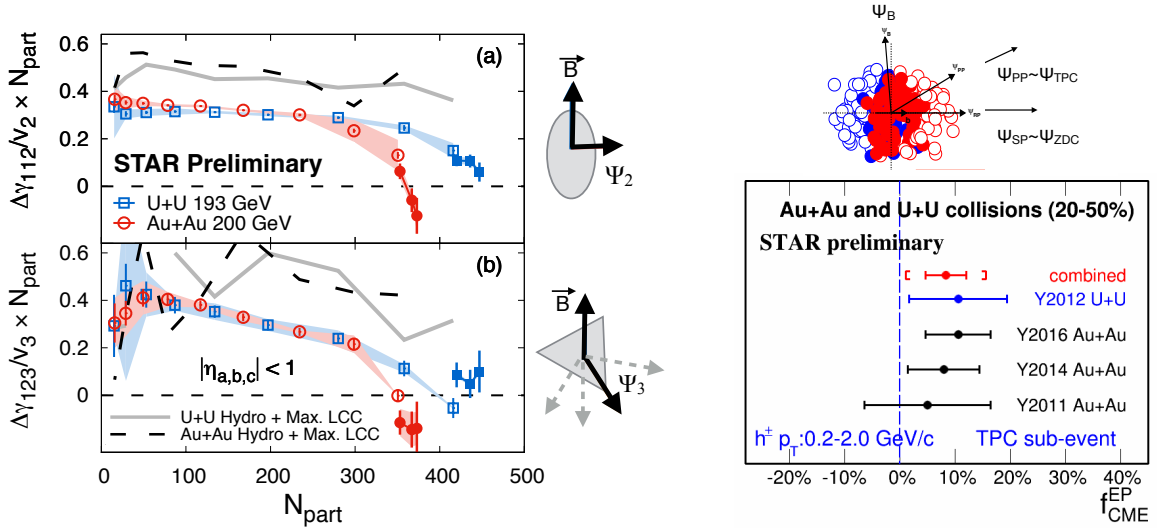


Figure 1. (Left) Measurement of charge separation along second and third order event planes in Au+Au and U+U collisions. (Right) Fraction of possible CME signal in the measurement of $\Delta\gamma$ with respect to spectator and participant planes [27].

183 with Au+Au and U+U data. It turns out that the possible sources of short range correlations
 184 due to photon conversion of $e^+ - e^-$, HBT and Coulomb effects can be identified and described as
 185 Gaussian peaks at small $\Delta\eta_{ab}$, the width and magnitude of which strongly depend on centrality
 186 and system size. Going to more peripheral centrality bins it becomes harder and harder to
 187 identify such components as they overlap with sources of di-jets fragmentation that dominate
 188 both same-sign and opposite sign correlations. An effort to decompose different components of
 189 $\Delta\gamma$ via study of $\Delta\eta_{ab}$ can be challenging although a clear sign of different sources of correlations
 190 are visible in change of shape of individual same-sign and opposite sign measurements of γ -
 191 correlator [26].

192 In any case, these differential measurements of $\Delta\gamma$ in isobar collisions provide the prospect
 193 to extract the $m_{inv}(\pi^+ + \pi^-)$ and $\Delta\eta$ dependence of CME signals that will provide much deeper
 194 insights on the origin of the effect.

195 6. Mixed harmonics measurements with second and third order event planes

196 In order to proceed in this section it is better to rewrite the conventional γ -correlator by a more
 197 general notation as $\gamma_{112} = \langle \cos(\phi_a^\alpha + \phi_b^\beta - 2\Psi_2) \rangle$. The idea is to measure charge separation across
 198 the third harmonic event plane by constructing a new correlator $\Delta\gamma_{123} = \gamma_{123}(OS) - \gamma_{123}(SS)$,
 199 where $\gamma_{123} = \langle \cos(\phi_a^\alpha + 2\phi_b^\beta - 3\Psi_3) \rangle$ that was introduced by CMS collaboration in Ref [13].
 200 Since the Ψ_3 plane is random and not correlated to B-field direction (see Fig.1), γ_{123} is purely
 201 driven by non-CME background, the contribution of which should go as v_3/N . This is very
 202 useful to contrast signal and background scenario by comparing the measurements in two
 203 isobaric collision systems. Since Ru+Ru has larger B-field than Zr+Zr but have comparable
 204 background, the case for CME would be as follows: $(\Delta\gamma_{112}/v_2)^{Ru+Ru}/(\Delta\gamma_{112}/v_2)^{Zr+Zr} > 1$ and
 205 $(\Delta\gamma_{112}/v_2)^{Ru+Ru}/(\Delta\gamma_{112}/v_2)^{Zr+Zr} > (\Delta\gamma_{123}/v_3)^{Ru+Ru}/(\Delta\gamma_{123}/v_3)^{Zr+Zr}$. Fig.1 (left) shows the
 206 measurement of these observables in U+U and Au+Au collisions. Within the uncertainties of
 207 the measurements no significant difference in the trend of $\Delta\gamma_{112}/v_2$ and $\Delta\gamma_{123}/v_3$ is observed
 208 for the two collision systems except for the very central events. Predictions from hydrodynamic
 209 model calculations with maximum possible strength of local charge conservation [17] is shown

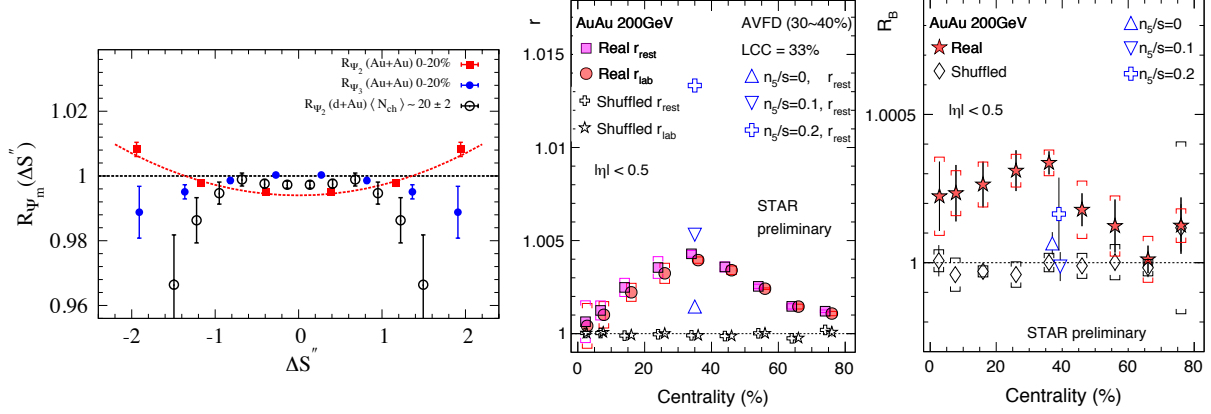


Figure 2. (Left) The R-observable shown for different collision systems, concave shape is consistent with CME expectation [24]. (Right) The two main quantities r and R_B derived from signed balance function, deviation from unity is consistent with CME expectation [30].

210 on the same plot. Overall observation indicates background dominate the measurements and a
 211 similar analysis of the isobar data is highly anticipated.

212 7. Charge separation along participant and spectator planes

213 This analysis makes use of the fact that B-field driven signal is more correlated to spectator
 214 plane in contrast to flow driven background which is maximum along the participant planes.
 215 The idea was first introduced in Ref [28] and later on followed up in Ref [29]. It requires
 216 measurement of $\Delta\gamma$ with respect to the plane of produced particles, a proxy for participant
 217 plane as well as with respect to the plane of spectators. In STAR the two can be done
 218 by using Ψ_2 from TPC and Ψ_1 from ZDC respectively. The approach is based on three
 219 main assumptions: 1) measured $\Delta\gamma$ has contribution from signal and background that can
 220 be expressed as $\Delta\gamma = \Delta\gamma^{bkg} + \Delta\gamma^{sig}$, 2) the background contribution to $\Delta\gamma$ should follow
 221 the scaling $\Delta\gamma^{bkg}(TPC)/\Delta\gamma^{bkg}(ZDC) = v_2(TPC)/v_2(ZDC)$ and, 3) the signal contribution to $\Delta\gamma$
 222 should follow the scaling $\Delta\gamma^{sig}(TPC)/\Delta\gamma^{sig}(ZDC) = v_2(ZDC)/v_2(TPC)$. The first two have been
 223 known to be working assumptions, widely used for a long time and can be used to test the case
 224 of CME [29] if $(\Delta\gamma/v_2)(ZDC)/(\Delta\gamma/v_2)(TPC) > 1$. The validity of the last one was studied and
 225 demonstrated in Ref [28]. Using all three equations one can extract [27] the fraction of possible
 226 CME signal $f_{CME} = \Delta\gamma^{sig}/\Delta\gamma$ in a fully data-driven way as shown in Fig.1(right). This analysis
 227 will be done with the isobar data and the case for CME will be $f_{CME}^{Ru+Ru} > f_{CME}^{Zr+Zr} > 0$.

228 8. Alternate measure: The novel R-observable

229 The R-observable is actually a distribution, introduced in Ref [22], and defined as the ratio of
 230 two distribution functions of the quantity ΔS parallel and perpendicular to B-field direction
 231 defined as $R_{\Psi_m}(\Delta S) = C_{\Psi_m}(\Delta S)/C_{\Psi_m}^\perp(\Delta S)$. Here ΔS measures the difference in the dipole
 232 moment of the positive and negative charge in an event (see Ref [22] for details). The shape of
 233 $R_{\Psi_2}(\Delta S)$ will be sensitive to CME as well as non-CME background whereas $R_{\Psi_3}(\Delta S)$ is purely
 234 driven by non-CME background and serves as a baseline. Model calculations have established
 235 several unique features of this observable: 1) presence of CME signal will lead to a concave
 236 shape of the $R_{\Psi_2}(\Delta S)$, 2) increasing strength of CME signal will increase the concavity of
 237 $R_{\Psi_2}(\Delta S)$, 3) in presence of CME, the concavity of $R_{\Psi_2}(\Delta S)$ will be larger than that of $R_{\Psi_3}(\Delta S)$.
 238 The measurement of R_{Ψ_m} is shown in Fig.2. The quantity $\Delta S''$ shown is a slight variant of

239 (ΔS) that incorporates correction for particle number fluctuations and event plane resolution.
 240 The observation of Fig.2 indicates more concave shape for R_{Ψ_2} compared to R_{Ψ_3} in Au+Au
 241 whereas flat or convex shapes for $p/d + Au$ indicating that the measurements are consistent
 242 with expectations of CME [24]. For isobar collisions the case of CME will be confirmed if: 1)
 243 a concave shape is observed for the ratio of the observables $R_{\Psi_2}(\Delta S)^{\text{Ru+Ru}}/R_{\Psi_2}(\Delta S)^{\text{Zr+Zr}}$ and
 244 2) the concavity should be weaker for $R_{\Psi_3}(\Delta S)^{\text{Ru+Ru}}/R_{\Psi_3}(\Delta S)^{\text{Zr+Zr}}$.

245 9. Alternate measure: The signed Balance function

246 A very recently proposed observable to search for CME is the signed balance function (SBF) [23].
 247 The idea is to account for the ordering of the momentum of charged pairs measured by the width
 248 of SBF that is expected to be different for out-of-plane as compared to in-plane measurement
 249 captured in the ratio r_{lab} . In addition, one can also account for the boost due to collective
 250 expansion of the system that forces all pairs to move in the same direction and measure the
 251 ratio in pair's rest frame r_{rest} . In presence of CME the individual ratios as well as the double ratio
 252 $R_B = r_{\text{rest}}/r_{\text{lab}}$ is expected to be greater than unity. The preliminary measurements shown in
 253 Fig.2 (right) from STAR in Au+Au 200 GeV seems to be consistent with CME expectation. This
 254 observable will be studied with the isobar data in STAR but not as a part of the blind analysis and
 255 the CME expectation will be: 1) $r(\text{Ru} + \text{Ru}) > r(\text{Zr} + \text{Zr})$, and 2) $R_B(\text{Ru} + \text{Ru}) > R_B(\text{Zr} + \text{Zr})$.

256 10. Steps for blind analysis of the isobar data from STAR

257 10.1. Modality of isobar running at RHIC

258 It is better to start with a short background on the activities that preceded the isobar blind
 259 analysis in STAR. The idea of colliding isobar, particularly Ru+Ru and Zr+Zr to make a decisive
 260 test of CME was proposed by Voloshin in Ref [31], the same paper which also proposed to use
 261 Uranium collisions to disentangle signal and background of CME. The possible difference in the
 262 signals relies on 10 – 18% higher B-field in Ru+Ru compared to Zr+Zr [32] in contrast to about
 263 4% difference in flow driven background [17]. Such estimates are sensitive to details of shapes,
 264 charge distribution and neutron skin thickness of the two isobar nuclei [32, 33, 34]. In the 2017-
 265 18 RHIC beam user request [35] STAR collaboration therefore proposed to collect data for two
 266 3.5 week runs in the year 2018. The projection was based on the prospect of achieving five-sigma
 267 significance or better in a scenario where the measurement of $\Delta\gamma$ has 80% non-CME background.
 268 This however corresponds to the fact that the systematic uncertainty in the measurements has
 269 to be within a few percent and below the statistical significance of the measurements, something
 270 that has never been attempted before in the correlation measurements from STAR or by other
 271 heavy-ion collision experiment in recent times to the best of my knowledge. This started a large
 272 scale collaboration wide effort in synergy with the RHIC collider accelerator department to plan
 273 for the isobar running in the year 2018. Based on the studies of previous years of data from
 274 $Au + Au$ and $U + U$ collisions several major sources of systematics in the measurement of $\Delta\gamma$
 275 were identified. The major sources include: run-to-run variation of detector response due to
 276 loss of acceptance, change in efficiency and variation in luminosity that affects the number of
 277 reconstructed tracks in the Time Projection Chamber. This eventually leads to uncorrectable
 278 systematic uncertainties in $\Delta\gamma$. In order to minimize such systematics the proposal were to: 1)
 279 switch species in RHIC between stores e.g., in orders like Ru+Ru, Zr+Zr, Ru+Ru and so on
 280 and, 2) keep long stores to level the luminosity aiming for specific rates in the coincidence
 281 measurements of beam fragments by the STAR zero-degree calorimeters. The aim was to
 282 maintain exact balance of run and detector conditions for the two species so that observations
 283 in the two systems are equally affected and can later on be largely eliminated in the ratios of
 284 observables.

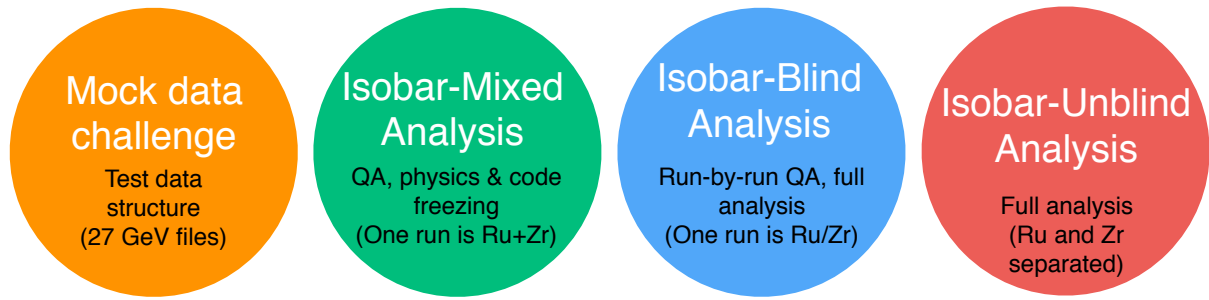


Figure 3. The steps of isobar blind analysis. This cartoon is based on the procedure for the blind analysis of isobar data that have been outlined in Ref [36].

285 *10.2. Blinding of data sets and preparation for analysis*

286 With the successful conclusion of the isobar run in the year 2018 STAR experiment collected
 287 more than 3 billion events for each isobar species. The next step was to develop the plans for a
 288 blind analysis, the main idea behind which is to eliminate predetermined biases. A total of five
 289 institutional groups are expected to perform the analysis of the data. The analysts from each
 290 group will focus on a specific aspect of the analysis described in the previous section although
 291 in many cases there are substantial overlap in some analyses that will help cross check the
 292 results. An important part of the blind analysis is the blinding of the data. The details of the
 293 blinding of the data structure is decided by members of a blinding-committee who are not part
 294 of the team of analysts and will work in close collaboration with STAR experts who are part
 295 of the production team. The idea is to provide the analysts the access to data in files where
 296 species-specific information are disguised or removed before the final step of unblinding. A
 297 careful consideration is taken by the blinding-committee to make sure the essential information
 298 available to do the analysis specific quality assurance of the data by the analysts. Some of
 299 the quality assurance, calibration and centrality determination that require species information
 300 are done only by STAR experts who are not a part of the team of analysts. Above all, the
 301 main goal of the committee is to make sure that under no circumstances physics analysts can
 302 access un-blinded data that can jeopardize the blind analysis. For example, all the data sets
 303 are produced with pseudo-run-number that cannot be used by the analysts to retrieve the exact
 304 species information.

305 *10.3. Methods for the isobar blind analysis*

306 The detailed procedure for the blind analysis of isobar data have been outlined in Ref [36].
 307 Figure.3 is a cartoon that summarizes the four steps and the main idea.

308 In the zeroth step shown in (by orange circle) the extreme left of Fig.3 is the mock data
 309 challenge which is not exactly a step of the isobar data analysis but a crucial step to familiarize
 310 the analysts with the technicalities of the data structures that have been specifically designed
 311 for blind analysis.

312 The first step shown in Fig.3 (by green circle) as the “isobar-mixed analysis” or “mixed-blind
 313 analysis” is truly the first step of blind analysis. This is also the most challenging steps from
 314 the point of view of the analysts. In this step the analysts are provided with data sample where
 315 each run comprise of events that are “mix” samples from two species. In this step the analysts
 316 perform the full quality assurance (QA) and physics analysis of the data, document every details
 317 of steps of the procedure and freeze the codes. After the completion of this step no changes
 318 to the analysis code is permissible. Also, no changes in the analysis procedure is allowed. The
 319 only permissible change in the following step is to reject bad runs or pile-up events. However,
 320 in order to avoid predetermined bias in analysis such rejection cannot be done arbitrarily and

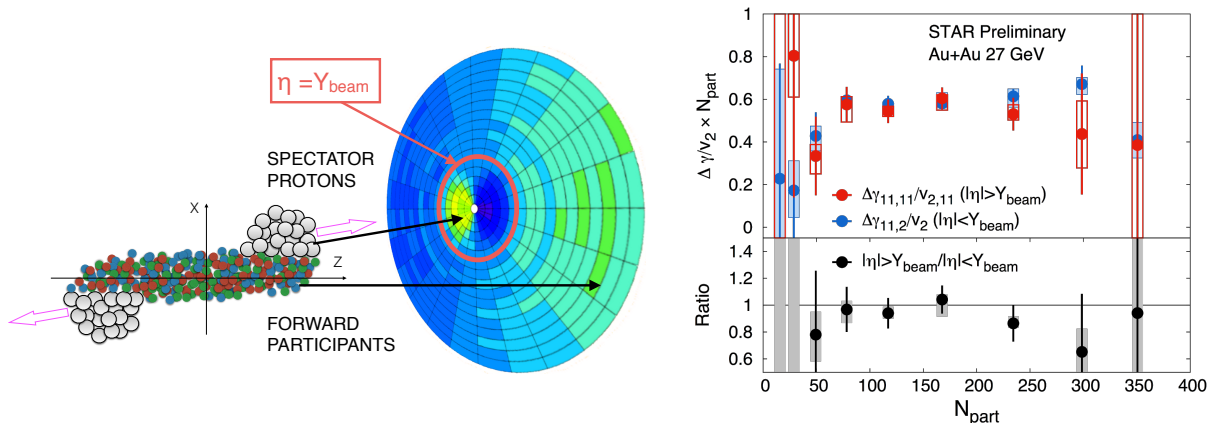


Figure 4. (Left) Figure showing EPD detector acceptance cover beam rapidity and detecting both forward participants and spectators in 27 GeV Au+Au collisions. (Right) γ -correlators scaled by v_2 across different event-planes and double ratio of spectators/participant event planes which should be unity for no-CME scenario.

321 an automated algorithm must be developed in this step and the related codes have to be frozen.
 322 The stability of the automated QA algorithm is tested with some of the existing data sets of
 323 Au+Au and U+U collisions.

324 The second step shown in Fig.3 (by blue circle) is referred to as the “isobar-blind analysis”
 325 or “unmixed-blind analysis”. From this step on-wards the analysts are allowed to run their
 326 previously frozen codes. The main purpose of this step is to perform run-by-run QA of the
 327 data sample. For this the analysts are provided with files each of which contain data from
 328 a single species that is either Ru or Zr. However, there are two conditions: the files contain
 329 limited number of events that cannot lead to any statistically significant result and the species
 330 information is not revealed. Although a pseudo-run-number is used for each file, the time
 331 ordering is preserved with a unique mapping that is unknown to the analysts. It is important to
 332 maintain the time ordering to identify time-dependent changes in detectors and run conditions
 333 as a part of the run-by-run quality assurance. With this limited data sample the analysts need
 334 run the frozen automated algorithm to identify bad runs. A similar automated algorithm is also
 335 used for identifying and rejecting bad runs. After this step no more changes are allowed in terms
 336 of QA.

337 The final step of isobar blind analysis is shown by red circle in Fig.3 is referred to as “isobar-
 338 unblind” analysis. In this step the species information will be revealed and the physics results
 339 will be produced by the analysts using the previously frozen codes. The finding from this step
 340 will be directly be submitted for publication without any kind of alteration. If a mistake is
 341 found in the analysis code, the erroneous results will also accompany the corrected results.

342 11. Post-isobar era and prospects for CME search at lower collision energies

343 Regardless of the outcome of the measurements with the isobar program, that will be performed
 344 at the top RHIC energy, one question will remain. What happens at lower collision energy? In
 345 this context a new idea has emerged. The newly installed event-plane detector (EPD) upgrade
 346 provides a new capability at STAR towards CME search at lower collision energy and for the
 347 Beam Energy Scan phase-II program [37]. The idea is simple, at lower energies EPD acceptance
 348 ($2.1 < |\eta| < 5.1$) falls in the region of beam rapidity (Y_{beam}) and can measure the plane of strong
 349 directed flow (Ψ_1) of spectator protons, beam fragments and stopped protons, therefore strongly
 350 correlated to the B-field direction (See fig4). The next step is to measure $\Delta\gamma$ with respect to

351 Ψ_1 and compare it with the measurement of $\Delta\gamma$ along Ψ_2 planes from outer regions of EPD
352 and TPC at mid-rapidity that are weakly correlated to the B-field directions. A test of CME
353 scenario will be to see if large difference is observed in the measurements. First preliminary
354 measurements from STAR as shown in Fig 4 is dominated by uncertainty but seems to show a
355 lot of prospects for the CME search at lower energies.

356 12. Summary

357 Despite several challenges experimental efforts have been continued towards disentangling the
358 CME signals from non-CME background in the measurement of charge separation across reaction
359 plane. The highly anticipated results from the blind analysis of isobar collisions data provides
360 us the best opportunity to make a decisive test of the CME in heavy-ion collisions.

361 13. Reference

- 362 [1] Kharzeev D and Pisarski R D 2000 *Phys.Rev.* **D61** 111901 (*Preprint hep-ph/9906401*)
- 363 [2] Kharzeev D 2006 *Phys.Lett.* **B633** 260–264 (*Preprint hep-ph/0406125*)
- 364 [3] Voloshin S A 2004 *Phys. Rev.* **C70** 057901 (*Preprint hep-ph/0406311*)
- 365 [4] Abelev B I *et al.* (STAR) 2009 *Phys. Rev. Lett.* **103** 251601 (*Preprint 0909.1739*)
- 366 [5] Abelev B I *et al.* (STAR) 2010 *Phys. Rev.* **C81** 054908 (*Preprint 0909.1717*)
- 367 [6] Abelev B *et al.* (ALICE) 2013 *Phys. Rev. Lett.* **110** 012301 (*Preprint 1207.0900*)
- 368 [7] Adamczyk L *et al.* (STAR) 2013 *Phys. Rev.* **C88** 064911 (*Preprint 1302.3802*)
- 369 [8] Adamczyk L *et al.* (STAR) 2014 *Phys. Rev.* **C89** 044908 (*Preprint 1303.0901*)
- 370 [9] Adamczyk L *et al.* (STAR Collaboration) 2014 *Phys.Rev.Lett.* **113** 052302 (*Preprint 1404.1433*)
- 371 [10] Adam J *et al.* (ALICE) 2016 *Phys. Rev.* **C93** 044903 (*Preprint 1512.05739*)
- 372 [11] Khachatryan V *et al.* (CMS) 2016 *Phys. Rev. Lett* [Phys. Rev. Lett.118,122301(2017)] (*Preprint 1610.00263*)
- 373 [12] Acharya S *et al.* (ALICE) 2018 *Phys. Lett.* **B777** 151–162 (*Preprint 1709.04723*)
- 374 [13] Sirunyan A M *et al.* (CMS) 2018 *Phys. Rev.* **C97** 044912 (*Preprint 1708.01602*)
- 375 [14] Adam J *et al.* (STAR) 2019 *Phys. Lett. B* **798** 134975 (*Preprint 1906.03373*)
- 376 [15] Adam J *et al.* (STAR) 2020 (*Preprint arXiv:2006.05035*)
- 377 [16] Pratt S 2010 (*Preprint 1002.1758*)
- 378 [17] Schenke B, Shen C and Tribedy P 2019 *Phys. Rev.* **C99** 044908 (*Preprint 1901.04378*)
- 379 [18] Jiang Y, Shi S, Yin Y and Liao J 2018 *Chin. Phys. C* **42** 011001 (*Preprint 1611.04586*)
- 380 [19] Belmont R and Nagle J 2017 *Phys. Rev. C* **96** 024901 (*Preprint 1610.07964*)
- 381 [20] Schenke B, Shen C and Tribedy P 2020 *Phys. Lett. B* **803** 135322 (*Preprint 1908.06212*)
- 382 [21] Kharzeev D, Tu Z, Zhang A and Li W 2018 *Phys. Rev. C* **97** 024905 (*Preprint 1712.02486*)
- 383 [22] Magdy N, Shi S, Liao J, Ajitanand N and Lacey R A 2018 *Phys. Rev. C* **97** 061901 (*Preprint 1710.01717*)
- 384 [23] Tang A 2020 *Chin. Phys. C* **44** 054101 (*Preprint 1903.04622*)
- 385 [24] Adam J *et al.* (STAR) 2020 (*Preprint arXiv:2006.04251*)
- 386 [25] Zhao J, Li H and Wang F 2019 *Eur. Phys. J. C* **79** 168 (*Preprint 1705.05410*)
- 387 [26] Tribedy P (STAR) 2017 *Nucl. Phys. A* **967** 740–743 (*Preprint 1704.03845*)
- 388 [27] Zhao J (STAR) 2020 (*Preprint 2002.09410*)
- 389 [28] Xu H j, Zhao J, Wang X, Li H, Lin Z W, Shen C and Wang F 2018 *Chin. Phys.* **C42** 084103 (*Preprint*
390 *1710.07265*)
- 391 [29] Voloshin S A 2018 *Phys. Rev.* **C98** 054911 (*Preprint 1805.05300*)
- 392 [30] Lin Y (STAR) 2020 (*Preprint 2002.11446*)
- 393 [31] Voloshin S A 2010 *Phys. Rev. Lett.* **105** 172301 (*Preprint 1006.1020*)
- 394 [32] Deng W T, Huang X G, Ma G L and Wang G 2018 *Phys. Rev. C* **97** 044901 (*Preprint 1802.02292*)
- 395 [33] Xu H J, Wang X, Li H, Zhao J, Lin Z W, Shen C and Wang F 2018 *Phys. Rev. Lett.* **121** 022301 (*Preprint*
396 *1710.03086*)
- 397 [34] Hammelmann J, Soto-Ontoso A, Alvioli M, Elfner H and Strikman M 2019 (*Preprint 1908.10231*)
- 398 [35] STAR 2017 BUR https://drupal.star.bnl.gov/STAR/system/files/STAR_BUR_Run1718_v22_0.pdf
- 399 [36] Adam J *et al.* (STAR) 2019 (*Preprint 1911.00596*)
- 400 [37] Adams J *et al.* 2019 (*Preprint 1912.05243*)